Effective conductivity of composites containing spheroidal inclusions: Comparison of simulations with theory

In Chan Kim
Department of Production and Mechanical Engineering, Kunsan National University, Kunsan, Chollabuk-Do Seoul, Korea

S. Torquato[a)]
Princeton Materials Institute and Department of Civil Engineering and Operations Research, Princeton University, Princeton, New Jersey 08544

(Received 25 January 1993; accepted for publication 15 April 1993)

We determine, by first-passage-time simulations, the effective conductivity tensor σ_e of anisotropic suspensions of aligned spheroidal inclusions with aspect ratio b/a. This is a versatile model of composite media, containing the special limiting cases of aligned disks ($b/a=0$), spheres ($b/a=1$), and aligned needles ($b/a=\infty$), and may be employed to model aligned, long- and short-fiber composites, anisotropic sandstones, certain laminates, and cracked media. Data for σ_e are obtained for prolate cases ($b/a=2$, 5, and 10) and oblate cases ($b/a=0.1$, 0.2, and 0.5) over a wide range of inclusion volume fractions and selected phase conductivities (including *superconducting* inclusions and *perfectly insulating* "voids"). The data always lie within second-order rigorous bounds on σ_e due to Willis [J. Mech. Phys. Solids **25**, 185 (1977)] for this model. We compare our data for prolate and oblate spheroids to our previously obtained data for spheres [J. Appl. Phys. **69**, 2280 (1991)].

I. INTRODUCTION

Transport and mechanical properties of composites containing inclusions have become a topic of great interest in recent years due, in part, to new and powerful theoretical methods that have been developed to predict effective properties[1–3] and because of the manifest technological importance of such materials. For example, fibrous dispersions are employed in a host of applications, including insulation, sports equipment, automobiles, and aircraft. Packed beds and solids containing distributions of cracks are other important types of heterogeneous materials that are modeled well as a composite containing inclusions. The preponderance of studies have attempted to predict the transport and mechanical properties of composites containing *spherical inclusions*.[3] Considerably less work has been carried out to determine the effective properties of anisotropic dispersions. (See Refs. 2–8 and references therein for examples of such anisotropic studies.)

In this paper, we consider determining the effective electrical (or thermal) conductivity tensor σ_e of anisotropic suspensions of aligned spheroids of arbitrary aspect ratio b/a which are mutually impenetrable. This is a useful model of statistically anisotropic heterogeneous media, containing the special limiting cases of oriented disks ($b/a=0$), spheres ($b/a=1$), and oriented needles ($b/a=\infty$), and may be generally employed to model aligned, long- and short-fiber composites, anisotropic sandstones, laminates, and cracked media. Virtually all previous investigations have dealt with the determination of σ_e for oriented spheroids using theoretical methods. There are few *rigorous* results for this model. Lu and Kim[7] have obtained σ_e for dilute, *superconducting* dispersions exactly through second order in the spheroid concentration. Willis[4] and, subsequently, Torquato and Lado[8] have derived rigorous bounds on σ_e for spheroidal suspensions for *arbitrary phase conductivities*. To our knowledge, there are no determinations of σ_e for this versatile model obtained from computer simulations. Such computer experiments could be used to provide tests on theoretical predictions of the conductivity tensor σ_e.

The effective conductivity tensor σ_e for aligned spheroidal dispersions is determined here by generalizing the efficient first-passage-time algorithm developed by the authors[9–11] to compute the conductivity of isotropic dispersions. We will compute σ_e for a wide range of aspect ratios ($0.1 \leqslant b/a \leqslant 10$). Although we will primarily examine cases where the inclusions of conductivity σ_2 are more conducting than the matrix of conductivity σ_1 (i.e., $\sigma_2/\sigma_1 > 1$), including superconducting inclusions ($\sigma_2/\sigma_1=\infty$), we will also determine σ_e in the instances of perfectly insulating inclusions or "voids" ($\sigma_2/\sigma_1=0$). The case of superconducting inclusions is encountered commonly in applications such as in metal-enhanced plastics and graphite-enhanced plastics.[7] The great disparity in the thermal conductivities of metals (graphites) and plastics makes the filler essentially superconducting relative to the matrix. The instance of perfectly insulating voids is typical of cracks in solid bodies. Our simulation results will be compared to rigorous bounds. As is well known, by mathematical analogy, the results given here for σ_e translate immediately into equivalent results for effective dielectric constant, magnetic permeability, and diffusion coefficient associated with flow past obstacles.

In Sec. II we describe the first-passage-time equations for the case of a *statistically anisotropic* dispersions of isotropic inclusions in an isotropic matrix. Section III gives the simulation details. In Sec. IV we briefly discuss rigor-

[a)]Author to whom all correspondence should be addressed.

 0021-8979/93/74(3)/1844/11/$6.00

ous theories for predicting σ_e, present our results for σ_e for spheroidal suspensions, and compare them to rigorous bounds.

II. FIRST-PASSAGE-TIME FORMULATION

A Brownian-motion simulation technique to obtain "exactly" the effective conductivity for general multiphase isotropic composites was recently given by the authors.[9,10] The appropriate first-passage-time equations at the multiphase interface were derived to reduce significantly the computation time required to keep track of the mean square displacements of the Brownian trajectories. The technique was first employed to determine the effective conductivities σ_e of equilibrium distributions of two-dimensional hard disks.[9] The first-passage-time method was subsequently used to compute σ_e of three-dimensional equilibrium distributions of hard spheres[10] and of overlapping spheres.[11] As noted in Ref. 10, the formulation is general in that it can be extended to treat *macroscopically anisotropic* composites with effective conductivity tensor σ_e. Here we focus our attention on cases of *statistically anisotropic* media with isotropic phase conductivities. The method can also be extended to instances where the phases themselves possess anisotropy, but we shall not deal with such cases here.

A. Effective conductivity

Consider a Brownian particle (conduction tracer) moving in a *homogeneous* and *isotropic* medium of (scalar) conductivity σ. Since the mean hitting time $\tau(R^2)$, which is defined to be the mean time taken for a Brownian particle initially at the center of a d-dimensional sphere of radius R to hit the surface for the first time, is given by $\tau(R^2)=R^2/2d\sigma$ (see, e.g., Ref. 8), the conductivity σ itself of an infinite medium is expressed as[9]

$$\sigma=\left.\frac{R^2}{2d\tau(R^2)}\right|_{R^2\to\infty}. \tag{1}$$

Likewise, the (scalar) effective conductivity σ_e of a d-dimensional *isotropic composite* medium is expressed as

$$\sigma_e=\left.\frac{X^2}{2d\tau_e(X^2)}\right|_{X^2\to\infty}. \tag{2}$$

Here $\tau_e(X^2)$ is the total mean time associated with the total mean square displacement X^2 of a Brownian particle moving in the isotropic composite medium. For the effective conductivity tensor $\sigma_e=(\sigma_e)_{ij}$ of a d-dimensional *statistically anisotropic* medium, Eq. (2) is simply generalized as[10]

$$(\sigma_e)_{ij}=\left.\frac{X_iX_j}{2\tau_e(X^2)}\right|_{X^2\to\infty}, \tag{3}$$

where $(\sigma_e)_{ij}$ represents the elements of the second-rank, symmetric conductivity tensor σ_e and X_i $(i=1, 2,...,d)$ is the displacement of the Brownian particle in the ith direction such that $X^2=X_1^2+X_2^2+\cdots+X_d^2$. The quantity $\tau_e(X^2)$ is the total mean time associated with the total mean square displacement X^2 of a Brownian particle moving in the statistically anisotropic composite medium.

In the actual computer simulation, in most cases where the Brownian particle is far from the two-phase interface, we employ the time-saving first-passage time technique[12] which is now described. First, one constructs the largest imaginary concentric sphere of radius R around the Brownian particle which just touches the multiphase interface. The Brownian particle then jumps in *one step* to a random point on the surface of this imaginary sphere and the process is repeated, each time keeping track of R_k^2 (or, equivalently, the mean hitting time τ) where R_k is the radius of the kth first-passage sphere, until the particle is within some prescribed *very small* distance of two-phase interface. At this juncture, we need to compute not only the mean hitting time $\tau_s(R)$ associated with imaginary concentric sphere of radius R in the small neighborhood of the interface but also the probability of crossing the interface. Both of these quantities are functions of σ_1, σ_2 and the local geometry. Thus, the expression for the effective conductivity tensor used in practice is given by

$$(\sigma_e)_{ij}=\left.\frac{\langle X_iX_j\rangle}{2\langle\Sigma_k\tau_1(R_k^2)+\Sigma_l\tau_2(R_l^2)+\Sigma_m\tau_s(R_m^2)\rangle}\right|_{X^2\to\infty} \tag{4}$$

$$=\left.\frac{\langle X_iX_j\rangle}{2\langle\Sigma_k\tau_1(R_k^2)+\Sigma_l\tau_1(R_l^2)/\alpha+\Sigma_m\tau_s(R_m^2)\rangle}\right|_{X^2\to\infty}, \tag{5}$$

since $\tau_e(X^2)=\Sigma_k\tau_1(R_k^2)+\Sigma_l\tau_2(R_l^2)+\Sigma_m\tau_s(R_m^2)$, where $\tau_1(R)$ $[\tau_2(R)]$ denotes the mean hitting time associated with a *homogeneous* first-passage sphere of radius R of conductivity σ_1 $[\sigma_2]$ and $\alpha=\sigma_2/\sigma_1$ denotes the conductivity ratio. Here the summations over the subscripts k and l are for the Brownian paths in phase 1 and phase 2, respectively, the summation over the subscript m is for paths crossing the interface, and the angular bracket denotes an ensemble average. Thus, for any single Brownian trajectory, the time steps are variable depending on the size of the first-passage spheres.[9,12] The second equality (5) follows because the mean hitting time is inversely proportional to the conductivity [cf. Eq. (1)]. Equation (5) is the basic equation to be used to compute the effective conductivity tensor σ_e of statistically anisotropic distributions of inclusions.

B. Brownian particle crossing the interface

A Brownian particle moving in one phase of the statistically anisotropic medium eventually comes near the two-phase interface. Whenever the Brownian particle is close to the interface, the first-passage quantities, described below, should be determined.

Let $\Omega=\Omega_1\cup\Omega_2$ be the small spherical first-passage region of radius R centered at the interface, where Ω_i is the portion of Ω that is in phase i $(i=1, 2)$, and $\partial\Omega_i$ be the surface of Ω_i excluding the two-phase interface (see Fig. 1). The key questions are:

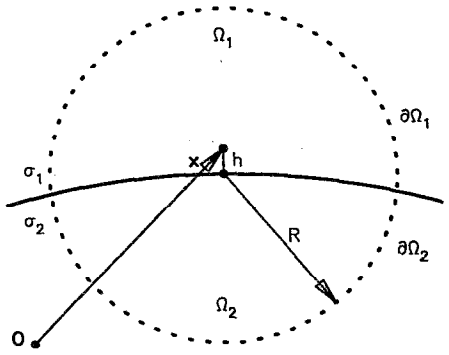

FIG. 1. Two-dimensional depiction of the small neighborhood of the curved interface between phase 1 of conductivity σ_1 and phase 2 of conductivity σ_2.

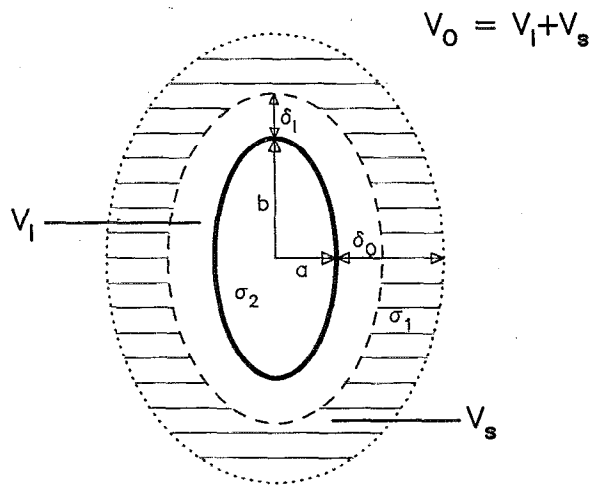

FIG. 2. Two-dimensional depiction of a superconducting spheroid ($\alpha=\sigma_2/\sigma_1$) of aspect ratio b/a, where a is the semiaxis in the x and y directions and b is the semiaxis in the z direction. The spheroid is surrounded by two concentric shells of conductivity σ_1: one shell having thickness δ_I and the other shell having thickness δ_O. Here V_I is the volume of the spheroid plus the concentric shell of thickness δ_I and V_S is the volume of the concentric shell of thickness δ_O. $V_O=V_I+V_S$.

(i) What is the probability p_1 (p_2) that the Brownian particle initially at x near the two-phase interface eventually first arrives at the surface $\partial\Omega_1$ (the surface $\partial\Omega_2$)?

(ii) What is the mean hitting time τ_s for the Brownian particle initially at x to hit $\partial\Omega$ ($=\partial\Omega_1\cup\partial\Omega_2$) for the first time?

The authors[9,10] obtained the first-passage-time quantities p_i and τ_s as solutions of certain Laplace and Poisson boundary-value problems, respectively. Their results for p_1, p_2, and τ_s are summarized as follows:

$$p_1=\frac{A_1}{A_1+\alpha A_2}\left[1+O\left(\frac{h}{R}\right)\right], \tag{6}$$

$$p_2=1-p_1=\frac{\alpha A_2}{A_1+\alpha A_2}\left[1+O\left(\frac{h}{R}\right)\right], \tag{7}$$

and

$$\tau_s=\frac{R^2}{6\sigma_1}\frac{V_1+V_2}{V_1+\alpha V_2}\left[1+O\left(\frac{h}{R}\right)^2\right], \tag{8}$$

where A_i is the area of the surface $\partial\Omega_i$ in phase i ($i=1, 2$), V_i is the volume of region Ω_i, and h ($h/R\ll 1$) is the small distance of the Brownian particle from the interface. As noted in Ref. 11, first-passage Eqs. (6)–(8) are general in that they can be used for any shape of the two-phase interface.

C. Brownian particle at the surface of superconducting phase

Consider suspensions of superconducting spheroids ($\alpha=\infty$). It can be easily seen that for $\alpha=\infty$, Eqs. (6)–(8) immediately yield trivial answers: $p_1=0$, $p_2=1$, and $\tau_s=0$. This implies that the Brownian particle at the interface boundary always gets trapped in the superconducting phase and never escapes from there, spending no time in the process. This is undesirable from a simulation standpoint since we need to investigate the Brownian particle's behavior in the large-time limit. The authors[8] provided a first-passage-time technique for this special case $\alpha=\infty$, the essence of which is as follows: (i) A Brownian particle moves in the same fashion as the Brownian motion in the homogeneous region if it is in the nonsuperconducting region far from the interface boundary, (ii) once it is very close to the interface boundary (in practice, within a prescribed small distance from the interface boundary), it is absorbed into the superconducting region and jumps out of the superconducting region after spending time τ_s, (iii) if it happens to be inside the superconducting region (in the actual simulation, this can take place in choosing the random initial location of the Brownian particle), the procedure of (ii) is applied. Note that the computation of τ_s in step (ii) is the key to the technique and is now described below.

Figure 2 depicts a two-dimensional schematic diagram of a superconducting spheroid of aspect ratio b/a, where a is the semiaxis in the x and y directions and b is the semiaxis in z direction. In order to use the first-passage algorithm in such instances, we need to compute τ_s associated with the concentric composite spheroids whenever the Brownian particle is within a prescribed small distance δ_1 ($0<\delta_1\ll a$) from the interface. It is convenient to introduce here other length parameters, namely, δ_I and δ_O. In Fig. 2, δ_I is the actual distance of the Brownian particle from the interface boundary, and δ_O is the distance by which the Brownian particle is displaced from the interface boundary such that $0\leqslant\delta_I\leqslant\delta_1\leqslant\delta_O\leqslant\delta_2<a$. The distance δ_O is determined as the smaller of another prescribed distance δ_2 and the distance to the next nearest spheroid.

The authors[9] earlier provided an expression for τ_s for arbitrary-shaped inclusions, which is a generalization of the exact expression for spherical inclusions. Their expression for τ_s is convenient to use for complex inclusion shapes. However, for simple inclusion shapes, such as spheroids, we can compute exactly τ_s rather easily, as we describe now. The exact expression for τ_s for spheroidal inclusions is given by

TABLE I. The mean hitting time τ_1 for the Brownian particle initially at the center of the spheroid of semiaxes a and b to first hit the surface. 10^6 Brownian particles were used to determine τ_1 for prolate and oblate spheroids. We include the exact result for the case of a sphere, i.e., $\tau_1=a^2/6\sigma_1$.

	b/a	τ_1
	10	$0.249a^2/\sigma_1$
Prolate	5	$0.245a^2/\sigma_1$
	2	$0.222a^2/\sigma_1$
Sphere	1	$0.167a^2/\sigma_1$
	0.5	$0.0833a^2/\sigma_1$
Oblate	0.2	$0.0185a^2/\sigma_1$
	0.1	$0.00490a^2/\sigma_1$

$$\tau_s=\tau_1(a+\delta_O,b+\delta_O)-\tau_1(a+\delta_I,b+\delta_I)$$
$$=\tau_1(a,b)(\delta_O^2-\delta_I^2)/a^2, \tag{9}$$

as shown in the Appendix. Here $\tau_1(a,b)$ is the mean hitting time for a Brownian particle at the centroid of a spheroid of semiaxes a and b of conductivity σ_1, to first hit the surface of this spheroid. The quantity $\tau_1(a,b)$, which is given as a solution of certain differential equation,[9] can be easily determined by the first-passage algorithm described above in subsection A (see also the Appendix). Note that the computation of $\tau_1(a,b)$ for a homogeneous spheroid is much easier than the corresponding calculation for a composite spheroid. This is the basic calculation involved to compute the survival time in the context of diffusion-controlled reactions. The authors[12] earlier provided an efficient first-passage-algorithm to compute the survival time.

Thus, one needs to compute only $\tau_1(a,b)$ to determine τ_s. We determined $\tau_1(a,b)$ for each of the aspect ratios b/a we considered in this study by using 10^6 Brownian particles. The results for $\tau_1(a,b)$ are tabulated in Table I. Note that p_1 and p_2 are no longer relevant quantities in this case and therefore need not be computed.

III. SIMULATION PROCEDURE

Here we apply the first-passage-time technique to compute the effective conductivity σ_e of *equilibrium* distributions of nonoverlapping spheroidal inclusions aligned parallel to the x_3 axis with length $2b$ and maximum diameter $2a$. The inclusions have conductivity σ_2 and the matrix has conductivity σ_1. We consider cases of both conducting inclusions, i.e., $\alpha=\sigma_2/\sigma_1>1$, and perfectly insulating inclusions or "voids" ($\alpha=0$). We first describe the simulation procedure in some detail and then present our simulation results in the subsequent section.

Obtaining the effective conductivity σ_e of random heterogeneous media from computer simulations is a two-step process:

(i) First, one generates realizations of equilibrium distributions of the random heterogeneous medium.

(ii) Second, employing the first-passage-time technique, one determines the effective conductivity for each realization (using many Brownian particles) and then averages over a sufficiently large number of realizations to obtain σ_e.

Generating a realization of an equilibrium distribution of nonoverlapping spheres is relatively easily achieved by a standard Metropolis algorithm.[13] By an equilibrium distribution of nonoverlapping particles we mean configurations taken from an ensemble of hard-particle systems that are in thermal equilibrium. The generation of equilibrium configurations for nonspherical shapes, such as oriented spheroids, is generally considerably more involved. However, the generation of an equilibrium distribution of oriented spheroids is substantially simplified by exploiting the observation made by Lebowitz and Perram.[14] They observed that oriented spheroids of shape

$$\frac{(x^2+y^2)}{a^2}+\frac{z^2}{b^2}=1 \tag{10}$$

are converted into spheres of radius a at the same volume fraction by a scale transformation to coordinates

$$R\equiv(X,Y,Z)=[x,y,(a/b)z], \tag{11}$$

and thus the thermodynamics and particle correlations of oriented spheroids (whether nonoverlapping or overlapping) are reduced to the equivalent ones involving spheres. Here, X, Y, Z and x, y, z denote the coordinates in the sphere and spheroid domains, respectively. Therefore, the mapping

$$z=Z\left(\frac{b}{a}\right) \tag{12}$$

maps the Z coordinate in the sphere domain into the z coordinate in the corresponding spheroid domain. Torquato and Lado[8] used this scale transformation to compute the two-point matrix probability function S_2 for distributions of nonoverlapping oriented spheroids. Miller *et al.*[15] also used the same scale transformation to compute the trapping rate k of distributions of both nonoverlapping and overlapping oriented spheroidal traps.

We employ this transformation to generate equilibrium configurations of nonoverlapping oriented spheroids: the model of interest in the present study. We first generate equilibrium realizations of nonoverlapping spheres using the standard Metropolis algorithm[13] and then "stretch" (for $b/a>1$) or "compress" (for $b/a<1$) the entire system according to the mapping (12) to obtain corresponding distributions of nonoverlapping oriented spheroids of arbitrary aspect ratio b/a. N identical spheres of radius a are initially placed on lattice sites of a body-centered-cubical array in cubical cell of size L^3. The reduced number density $\eta=(N/L^3)(4\pi/3)a^3$ is then identical to the volume fraction of nonoverlapping spheroids ϕ_2. (However, in general, for interpenetrable spheroids, $\phi_2<\eta$.) The cell is surrounded by periodic images of itself. Each sphere is then randomly moved by a small distance to a new position which is accepted or not according to whether overlap occurs. This process is repeated until equilibrium is achieved. Once an equilibrium configuration of spheres is generated, the system is "stretched" or "compressed" us-

ing the mapping (12) such that the desired equilibrium configuration of nonoverlapping oriented spheroids is obtained. It is in the spheroid domain in which Brownian particles (conduction tracers) are released.

We now describe the details of the first-passage-time algorithm to compute the effective conductivity tensor $\boldsymbol{\sigma}_e$. The essence of the first-passage-time technique has been described in Sec. II. Here we need to be more specific about the conditions under which the Brownian particle is considered to be in the small neighborhood of the interface and hence when the mean time τ_s, and probabilities p_1 and p_2 need to be computed. An imaginary thin concentric shell of thickness δ_1 is drawn around each spheroid of semiaxes a and b.

We first describe the algorithm for the case of the distributions of nonsuperconducting ($\alpha < \infty$) spheroids. If a Brownian particle enters the aforementioned thin shell of thickness δ_1 surrounding a spheroid, then we employ the first-passage-time Eqs. (6)–(8), where the local phase surface area ratio A_2/A_1 and the local phase volume ratio V_2/V_1 of the imaginary sphere should be computed. If this imaginary first-passage sphere contains only a single, smooth interface boundary (as in Fig. 1), A_2/A_1 and V_2/V_1 are easily determined. However, if a Brownian particle is between two or more very closely located spheroids, then the imaginary first-passage sphere inevitably contains two or more interface boundaries. Computing A_2/A_1 and V_2/V_1 in such instances is nontrivial. In order to accomplish this, in the latter instances, we use the so-called *template method* introduced by the authors[11] to determine numerically the generally complex-shaped volume and area. An imaginary measuring template that has measuring points distributed uniformly and randomly is placed over the (volume or area) element of the two-phase medium to be measured. First, in order to compute A_2/A_1, we uniformly and randomly throw M_A points on the surface of the imaginary first-passage sphere of radius $R=\delta_2$, where δ_2 is another prescribed small distance such that $\delta_1 < \delta_2 < a$ and counts the number of occasions $M_{A,1}$ ($M_{A,2}$) that these points fall on $\partial\Omega_1$ ($\partial\Omega_2$) (see Fig. 1). The area ratio A_2/A_1 is then determined to be $M_{A,2}/M_{A,1}$. Next, M_V points are thrown inside the first passage sphere and the number of occasions $M_{V,1}$ ($M_{V,2}$) that these points fall in Ω_1 (Ω_2) is counted. The volume ratio V_2/V_1 is then determined to be $M_{V,2}/M_{V,1}$.

In cases of superconducting spheroids (see Fig. 2), the quantity τ_s associated with the superconducting spheroid of semiaxes a and b are determined by application of Eq. (9) in conjunction with Table I; see also the Appendix.

After a sufficiently large *total* mean square displacement, Eq. (4) is then employed to yield the effective conductivity for each Brownian trajectory and each realization. Many different Brownian trajectories are considered per realization. The effective conductivity tensor $\boldsymbol{\sigma}_e$ is finally determined by averaging the conductivities over all realizations. Finally, note that so-called Grid method[16] was used to reduce the computation time needed to check if the Brownian particle is near a spheroid. It enables one to check for spheroids in the immediate neighborhood of the Brownian particle instead of checking each spheroid.

In our simulations, we have taken $\delta_1=0.001$ and $\delta_2=0.03$ for nonsuperconducting spheroids ($\alpha=0$, 10) and $\delta_1=0.0001$ and $\delta_2=0.01$ for superconducting spheroids ($\alpha=\infty$). We considered 50–100 equilibrium realizations and 5–50 Brownian particles per realization, and have let the dimensionless total mean square displacement X^2/a^2 vary from 2 to 40, depending on the value of b/a, ϕ_2, and α. The aspect ratio b/a ranged from $b/a=0.1$ (disk or penny shapes) to $b/a=10$ (needles or slender rods). It should be appreciated that the wide range of parameters $(b/a,\phi_2,\alpha)$ that we wish to consider is rather ambitious in that it requires considerable computing time. For this reason, although we compute $\boldsymbol{\sigma}_e$ in the cases $\alpha=10$ and ∞ for aspect ratios $b/a=0.1$, 0.2, 0.5, 2, 5, and 10, we only provide data in the instance $\alpha=0$ for the extreme aspect ratios $b/a=0.1$ and 10. Our calculations were carried out on a VAX station 3100 and on a CRAY Y-MP.

IV. SIMULATION RESULTS AND DISCUSSION OF THEORY

A. Rigorous theories

Sen and Torquato[6] have derived two different types of perturbation expansions and rigorous bounds for the effective conductivity tensor $\boldsymbol{\sigma}_e$ of two-phase anisotropic composite media of arbitrary topology and dimensionality. One of these relations is an expansion in the difference in the phase conductivities whose nth-order tensor coefficients depend upon the set of n-point probability functions S_1, $S_2,\ldots,S_n$. The quantity $S_n(x_1,\ldots,x_n)$ gives the probability of finding n points at positions $x_1,\ldots,x_n$, respectively, simultaneously in one of the phases. Because it is generally difficult to determine S_n for $n\geqslant 5$, then such perturbation expansions will be useful only if the contrast difference is small. Through second order in the difference $(\alpha-1)$, the perturbation expansion yields[6]

$$\frac{\sigma_e}{\sigma_1}=\mathbf{U}+\phi_2\mathbf{U}(\alpha-1)-\phi_1\phi_2\mathbf{A}_2^*(\alpha-1)^2, \tag{13}$$

where $\mathbf{U}$ is the unit dyadic. $\mathbf{A}_2^*$ is the so-called "polarization" tensor which is an integral over S_2. In the special case of composite media containing spheroidal inclusions aligned parallel to the x_3 axis with length $2b$ and maximum diameter $2a$, one has[6,8]

$$\mathbf{A}_2^*=\begin{bmatrix} Q & 0 & 0 \\ 0 & Q & 0 \\ 0 & 0 & 1-2Q \end{bmatrix}, \tag{14}$$

where Q is

$$Q=\frac{1}{2}\left\{1+\frac{1}{(b/a)^2-1}\left[1-\frac{1}{2\chi_b}\ln\left(\frac{1+\chi_b}{1-\chi_b}\right)\right]\right\} \tag{15}$$

for prolate spheroids of aspect ratio $b/a>1$ and

$$Q=\frac{1}{2}\left\{1+\frac{1}{(b/a)^2-1}\left[1-\frac{1}{\chi_a}\tan^{-1}(\chi_a)\right]\right\} \tag{16}$$

for oblate spheroids of aspect ratio $b/a<1$. Here χ_a and χ_b are defined as

$$\chi_a^2=-\chi_b^2=(a^2/b^2)-1. \tag{17}$$

It is seen that $\mathbf{A}_2^*$, as well as the conductivity tensor σ_e for arbitrary α, is a diagonal, second-rank tensor with only two independent components: one parallel and the other perpendicular to the director of the system.

Lu and Kim[7] obtained the effective conductivity tensor σ_e for the special case of *superconducting* ($\alpha=\infty$), spheroidal inclusions exactly through second order in the inclusion volume fraction ϕ_2:

$$\frac{\sigma_e}{\sigma_1}=\mathbf{U}+\mathbf{b}_1\phi_2+\mathbf{b}_2\phi_2^2. \tag{18}$$

The coefficients $\mathbf{b}_n$ depend upon the n-particle statistics. Clearly, relation (18) is accurate only for *dilute* dispersions.

Willis[4] derived second-order rigorous bounds on σ_e for composites containing oriented spheroidal inclusions. Subsequently, these bounds were rederived by Torquato and Lado[8] using a different approach. These bounds are the only rigorous results capable of providing useful estimates of σ_e for spheroidal inclusions for arbitrary phase conductivities and volume fractions and may be stated in the notation of Ref. 8 as

$$\frac{\sigma_{\mathrm{L}}^{(2)}}{\sigma_1}\leqslant\frac{\sigma_e}{\sigma_1}\leqslant\frac{\sigma_{\mathrm{U}}^{(2)}}{\sigma_1}, \tag{19}$$

where

$$\frac{\sigma_{\mathrm{L}}^{(2)}}{\sigma_1}=[\mathbf{U}+(\phi_2\mathbf{U}+\phi_1\mathbf{A}_2^*)(\alpha-1)][\mathbf{U}+\phi_1\mathbf{A}_2^*(\alpha-1)]^{-1} \tag{20}$$

and

$$\frac{\sigma_{\mathrm{U}}^{(2)}}{\sigma_1}=[\alpha\mathbf{U}-(\phi_1\mathbf{U}+\phi_2\mathbf{A}_2^*)(\alpha-1)]\times[\mathbf{U}-\phi_2\mathbf{A}_2^*(1-1/\alpha)]^{-1}. \tag{21}$$

Here $\alpha>1$ and $\mathbf{A}_2^*$ is given by relation (14). The bounds (20) and (21) apply as well to anisotropic media of arbitrary microgeometry but $\mathbf{A}_2^*$ in this situation is not generally given by (14) but by an integral over S_2 (see Ref. 6). It is of interest to note that truncation of the *first* perturbation expansion derived by Sen and Torquato[6] after two-point terms yields the bounds (20) and (21).

The general form of bounds (20) and (21) are exactly realized for a variety of model composites,[17] one of which consists of *space-filling* inclusions of "singly coated" ellipsoids. The inner core is composed of phase 2 (phase 1) and the outer concentric shell is composed of phase 1 (phase 2) in the case of lower bound (20) [upper bound (21)]: the relative amount of each phase being determined by the volume fraction. These coated ellipsoids are all oriented in the same direction, but since they fill up the whole space, they appear in continuously varying sizes such that the ratio of their principal axes remain fixed. The general form of bounds (20) and (21) given in Ref. 6 are generalizations of the second-order Hashin–Shtrikman bounds and reduce to the latter in the macroscopically isotropic limit, i.e., when $\mathbf{A}_2^*=\mathbf{U}/3$. The correspondence between the bounds and the coated-ellipsoid geometries will be of use to us below where the bounds are compared to our data.

TABLE II. Diagonal components of the dimensionless effective conductivity for selected values of the spheroid volume fraction ϕ_2 and aspect ratio b/a at a phase conductivity ratio $\alpha=\sigma_2/\sigma_1=10$ as obtained from our first-passage-time simulations. Note that $(\sigma_e)_{11}/\sigma_1=(\sigma_e)_{22}/\sigma_1$. The data for spheres ($b/a=1$) are taken from our previous article.[a]

	$\alpha=10$					
	$(\sigma_e)_{11}/\sigma_1$			$(\sigma_e)_{33}/\sigma_1$		
b/a	$\phi_2=0.1$	$\phi_2=0.3$	$\phi_2=0.5$	$\phi_2=0.1$	$\phi_2=0.3$	$\phi_2=0.5$
0.1	1.60	3.26	5.00	1.12	1.45	2.05
0.2	1.47	2.78	4.39	1.13	1.48	2.09
0.5	1.37	2.11	3.35	1.18	1.63	2.35
1	1.25	1.93	3.02	1.25	1.93	3.02
2	1.23	1.78	2.65	1.41	2.53	3.85
5	1.22	1.74	2.61	1.71	3.21	4.87
10	1.19	1.73	2.59	1.81	3.48	5.20

[a]Reference 10.

B. Simulation results and comparison to rigorous bounds

Our simulation method has already been shown to yield the effective conductivity highly accurately for periodic as well as random suspensions for arbitrary dimensionality.[9,10] We will compare our conductivity simulation results for spheroidal suspensions to the bounds (19).

In the cases of conducting inclusions, we considered two conductivity ratios, i.e., $\alpha=10$ and $\alpha=\infty$, and the aspect ratios $b/a=0.1$, 0.2, 0.5, 2, 5, and 10. For the instances of insulating inclusions or voids, we studied the value of $\alpha=0$ for the extreme aspect ratios $b/a=0.1$ and $b/a=10$. Our data are summarized in Tables II–IV. Included in the tables are our previous results[10] for spheres ($b/a=1$).

Let us first consider the data for the case $\alpha=10$. Table II reveals that, at fixed volume fraction, the component

TABLE III. As in Table II, except for superconducting inclusions ($\alpha=\infty$). The data for spheres ($b/a=1$) are taken from our previous article.[a]

	$\alpha=\infty$					
	$(\sigma_e)_{11}/\sigma_1$			$(\sigma_e)_{33}/\sigma_1$		
b/a	$\phi_2=0.1$	$\phi_2=0.3$	$\phi_2=0.5$	$\phi_2=0.1$	$\phi_2=0.3$	$\phi_2=0.5$
0.1	3.61	19.44	53.75	1.18	2.29	3.62
0.2	2.30	7.11	22.69	1.24	2.32	3.70
0.5	1.51	3.35	6.88	1.28	2.36	3.81
1	1.34	2.48	4.78	1.34	2.48	4.78
2	1.27	2.06	3.50	1.68	3.60	8.26
5	1.25	1.99	3.46	3.13	10.12	25.42
10	1.23	1.90	3.33	9.03	36.36	99.64

[a]Reference 10.

$(\sigma_e)_{11}/\sigma_1$ $[=(\sigma_e)_{22}/\sigma_1]$ increases as the aspect ratio decreases (i.e., as the spheroid becomes more oblate). This is not surprising since as b/a approaches zero, the effective conductivity in the x_1-x_2 plane approaches that of resistance for conduction in parallel slabs of the two phases, i.e., $\sigma_e=\sigma_1\phi_1+\sigma_2\phi_2$. For the same reason, at fixed volume fraction, the component $(\sigma_e)_{33}/\sigma_1$ increases as the aspect ratio increases (i.e., as the spheroid becomes more prolate). Of course, the effective conductivity increases as the inclusion volume fraction ϕ_2 is increased, for fixed aspect ratio. Note that the effective conductivity for the extreme aspect ratios of $b/a=0.1$ (disk-like shapes) and $b/a=10$ (needle-like shapes) are within a factor of 2 of the data for spheres ($b/a=1$) at this moderate conductivity ratio.

Table III for superconducting inclusions ($\alpha=\infty$) shows that, at fixed volume fraction, the components $(\sigma_e)_{11}/\sigma_1$ and $(\sigma_e)_{33}/\sigma_1$ decrease and increase, respectively, as the aspect ratio is increased for the same reasons given above. Observe here, however, the the effective conductivity in the extreme aspect ratio cases can dramatically differ from the data for spheres. For example, the dimensionless effective conductivity $(\sigma_e)_{33}/\sigma_1$ for $b/a=10$ is about 20 times larger than for spheres.

In the case of perfectly insulating ($\alpha=0$) voids or "cracks," Table IV shows the same trends as reported above in the instances of conducting inclusions as far as dependence of the conductivity upon aspect ratio for fixed ϕ_2 is concerned. However, for $\alpha=0$, the effective conductivity is relatively insensitive to the aspect ratio, in contrast to the conducting-inclusions situations.

Figures 3 and 4 depict our conductivity data and the two-point bounds (20) and (21) for the oblate cases $b/a=0.5$ and $b/a=0.1$, respectively, with $\alpha=10$. In the case of Fig. 3, it is seen that the data for both diagonal components $(\sigma_e)_{11}/\sigma_1$ and $(\sigma_e)_{33}/\sigma_1$ lie closer to the lower

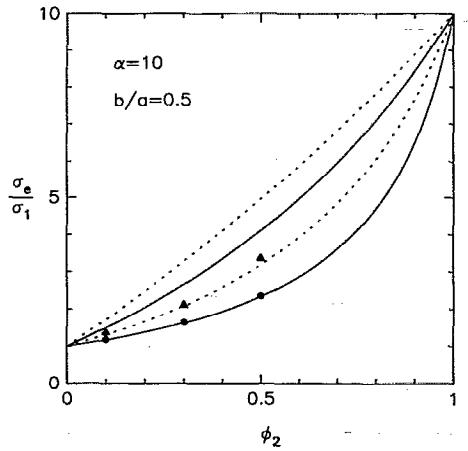

FIG. 3. The diagonal components of the dimensionless effective conductivity σ_e/σ_1 $[\sigma_e\equiv(\sigma_e)_{ii}]$ vs the inclusion volume fraction ϕ_2 for a composite containing aligned spheroids of aspect ratio $b/a=0.5$ and phase conductivity ratio $\alpha=\sigma_2/\sigma_1=10$. The dashed lines are the two-point bounds (see Refs. 4 and 8) (19) for $(\sigma_e)_{11}/\sigma_1=(\sigma_e)_{22}/\sigma_1$ and the triangles are our corresponding simulation data. The solid lines are the two-point bounds (see Refs. 4 and 8) for $(\sigma_e)_{33}/\sigma_1$ and the circles are our corresponding simulation data.

TABLE IV. As in Table II, except for perfectly insulating voids or "cracks" ($\alpha=0$). The data for spheres ($b/a=1$) are taken from our previous article.[a]

	$\alpha=0$					
	$(\sigma_e)_{11}/\sigma_1$			$(\sigma_e)_{33}/\sigma_1$		
b/a	$\phi_2=0.1$	$\phi_2=0.3$	$\phi_2=0.5$	$\phi_2=0.1$	$\phi_2=0.3$	$\phi_2=0.5$
0.1	0.887	0.653	0.415	0.496	0.183	0.068
1	0.856	0.602	0.381	0.856	0.602	0.381
10	0.819	0.526	0.308	0.898	0.692	0.489

[a]Reference 10.

bounds. (For a wide class of *isotropic* dispersions, it is well known that lower bounds can provide a good estimate of the effective conductivity when the inclusions are conducting; see Ref. 3 and references therein.) Recall that the lower bound corresponds to the aforementioned singly coated, space-filling, ellipsoidal geometry in which the inner core has conductivity σ_2. It is not hard to see that the actual spheroidal suspension corresponding to the data of Fig. 3, with its moderate degree of anisotropy and of phase conductivity contrast, is not significantly different than this singly coated ellipsoidal geometry, and thus the lower bound should provide a good estimate of the data. In the more anisotropic instance of Fig. 4, the lower bound for the 33 component gives a good estimate as well. However, the lower bound for the 11-component is accurate only at low inclusion volume fractions. The reason for this is that as ϕ_2 is increased, the actual highly anisotropic geometry begins to resemble more closely the singly coated ellipsoidal geometry corresponding to the upper bound (i.e., when the inner core has conductivity σ_1). It should also be noted that the 11-component bounds are rather tight.

In Figs. 5 and 6 we plot our data along with the two-point bounds for the prolate instances $b/a=2$ and $b/a=10$, respectively, with $\alpha=10$. Observe that the data again lie closer to the lower bounds. Note also that the 33-component bounds are very tight.

Figures 7 and 8 shows our conductivity data and the two-point lower bounds (20) for the oblate cases $b/a=0.5$

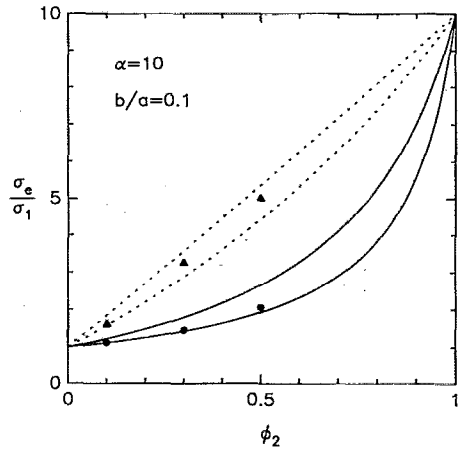

FIG. 4. As in Fig. 3, except with $b/a=0.1$.

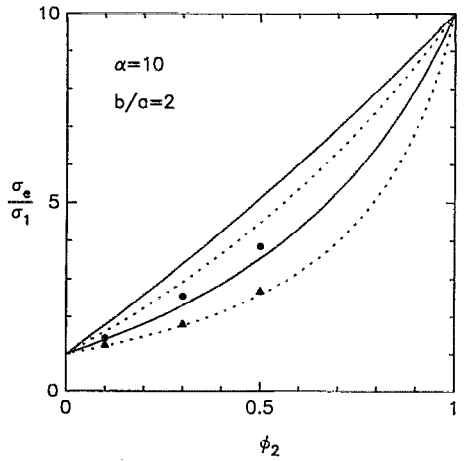

FIG. 5. As in Fig. 3, except with $b/a=2$.

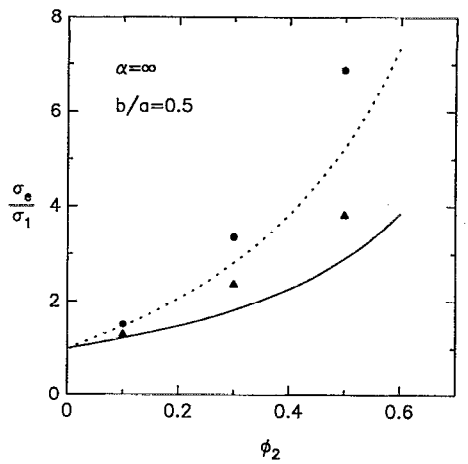

FIG. 7. The diagonal components of the dimensionless effective conductivity σ_e/σ_1 [$\sigma_e \equiv (\sigma_e)_{ii}$] vs the inclusion volume fraction ϕ_2 for a composite containing aligned spheroids of aspect ratio $b/a=0.5$ and phase conductivity ratio $\alpha=\sigma_2/\sigma_1=\infty$. The dashed line is the two-point lower bound (see Refs. 4 and 8) (20) for $(\sigma_e)_{11}/\sigma_1=(\sigma_e)_{22}/\sigma_1$ and the triangles are our corresponding simulation data. The solid line is the two-point lower bound (see Refs. 4 and 8) (20) for $(\sigma_e)_{33}/\sigma_1$ and the circles are our corresponding simulation data. The upper bounds diverge to infinity.

and $b/a=0.1$, respectively, with $\alpha=\infty$. The upper bounds diverge to infinity and the data still lie relatively close to the lower bounds, for reasons already noted. Whereas the bound for component $(\sigma_e)_{33}/\sigma_1$ for $b/a=0.5$ is sharp enough to provide a reasonable estimate of the data, the corresponding bound for the component $(\sigma_e)_{11}/\sigma_1$ is sufficiently accurate only at low volume fractions. For the penny-shaped case of $b/a=0.1$, the lower bound for $(\sigma_e)_{33}/\sigma_1$ provides a better estimate of the data than does the corresponding bound for $(\sigma_e)_{11}/\sigma_1$. Indeed, except at low inclusion volume fractions, the lower bound on $(\sigma_e)_{11}/\sigma_1$ significantly underestimates the data. The reason for such a large discrepancy at large volume fractions is that in the actual composite (which is highly anisotropic) the penny-shaped inclusions can be arbitrarily close to one another. The average interparticle separation (in the x_3 direction) is appreciably smaller than the corresponding separation in the singly coated ellipsoidal geometry of the lower bound (where the inclusions are always "well separated" as a result of possessing a concentric coating of conductivity σ_1) at large ϕ_2. Thus, conduction in the x_3 direction is greater in the actual composite than in the singly coated ellipsoidal geometry.

In Figs. 9 and 10 we plot our data along with the two-point bounds for the prolate instances $b/a=2$ and $b/a=10$, respectively, with $\alpha=\infty$. Generally speaking, since the upper bounds diverge to infinity, it is clear that the data lie relatively close to the lower bounds. In contrast to the oblate cases depicted in Figs. 7 and 8, the lower bounds on the component $(\sigma_e)_{11}/\sigma_1$ provide a better estimate of the data than does the corresponding bound for $(\sigma_e)_{33}/\sigma_1$. Again, this can be explained by appealing to the exact singly coated ellipsoidal geometries realized by the bounds.

Figures 11 and 12 show our data and the two-point upper bounds (21) for the extreme oblate case $b/a=0.1$ (disk-like shape) and the extreme prolate case $b/a=10$ (needle-like shape), respectively, with $\alpha=0$. Here the

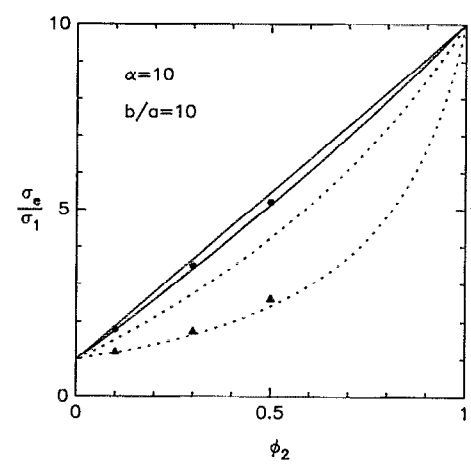

FIG. 6. As in Fig. 3, except with $b/a=10$.

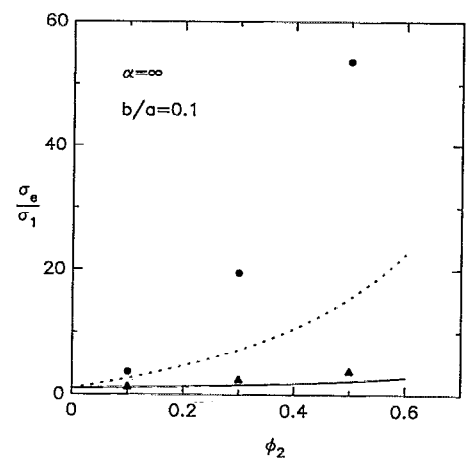

FIG. 8. As in Fig. 7, except with $b/a=0.1$.

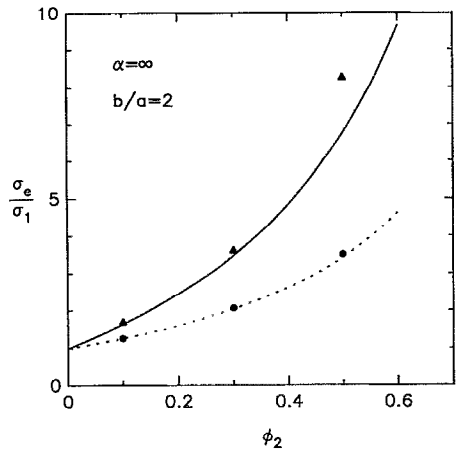

FIG. 9. As in Fig. 8, except with $b/a=2$.

lower bounds vanish identically and it is the upper bounds (corresponding to the singly coated geometry having an inner core of conductivity σ_2) that provide a good estimate of the effective conductivity.

To illustrate the dependence of the effective conductivity on aspect ratio b/a (for fixed volume fraction), we have plotted in Figs. 13 and 14 the 33 and 11 components of the conductivity tensor, respectively, versus $\log(b/a)$ for superconducting inclusions ($\alpha=\infty$) at a volume fraction $\phi_2=0.1$. Note that as b/a increases beyond unity the conductivity in the 33 direction increases precipitously. On the other hand, as $b/a\to 0$, the conductivity asymptotes to a constant value. In this limit, the lower bound predicts this constant to be ϕ_2^{-1}, which is in good agreement with Fig. 13. At high volume fractions (e.g., $\phi=0.5$, not shown), the bound does not accurately predict the true asymptote. Figure 14 shows the corresponding plot of the 11 component of the conductivity tensor. Here the conductivity approaches a constant value as $b/a\to\infty$; whereas as $b/a\to 0$, the conductivity rises sharply but not as steeply as the 33 component when $b/a\to\infty$.

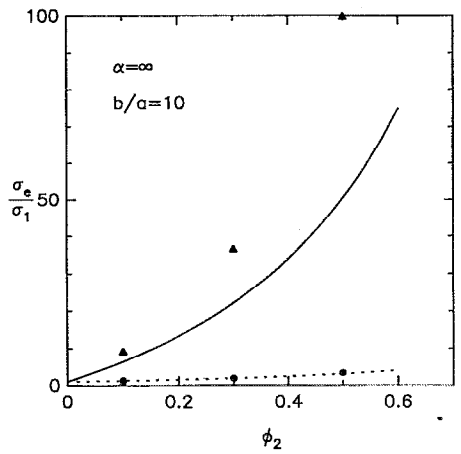

FIG. 10. As in Fig. 9, except with $b/a=10$.

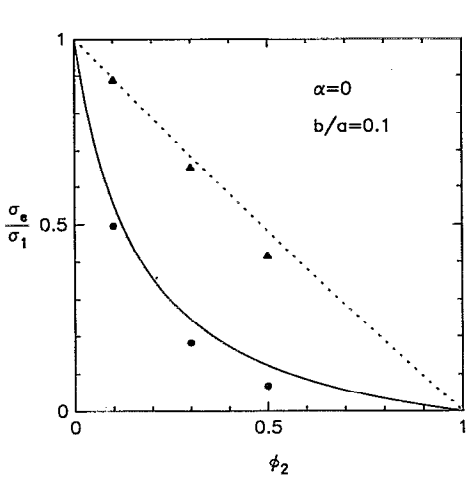

FIG. 11. The diagonal components of the dimensionless effective conductivity σ_e/σ_1 [$\sigma_e \equiv (\sigma_e)_{ii}$] vs the inclusion volume fraction ϕ_2 for a composite containing aligned spheroids of aspect ratio $b/a=0.1$ and phase conductivity ratio $\alpha=\sigma_2/\sigma_1=0$. The dashed line is the two-point upper bound (see Refs. 4 and 8) (21) for $(\sigma_e)_{11}/\sigma_1=(\sigma_e)_{22}/\sigma_1$ and the triangles are our corresponding simulation data. The solid line is the two-point upper bound (see Refs. 4 and 8) (21) for $(\sigma_e)_{33}/\sigma_1$ and the circles are our corresponding simulation data.

ACKNOWLEDGMENT

The authors gratefully acknowledge the support of the Office of Basic Energy Sciences, U.S. Department of Energy, under Grant No. DE-FG02-92ER14275.

APPENDIX: MEAN HITTING TIME FOR A SUPERCONDUCTING SPHEROID

Consider a Brownian particle (conduction tracer) at the *centroid* of a concentric composite spheroid where an inner superconducting ($\alpha=\infty$) spheroid of semiaxes a and b is surrounded by a nonsuperconducting concentric shell of thickness δ_O that has a conductivity σ_1 (see Fig. 2). The mean hitting time for such a Brownian particle to first hit the outer boundary of the resultant composite spheroid of semiaxes $a+\delta_O$ and $b+\delta_O$ is simply given by

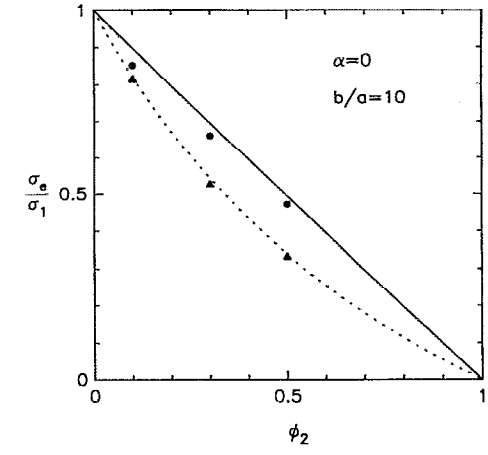

FIG. 12. As in Fig. 11, except with $b/a=10$.

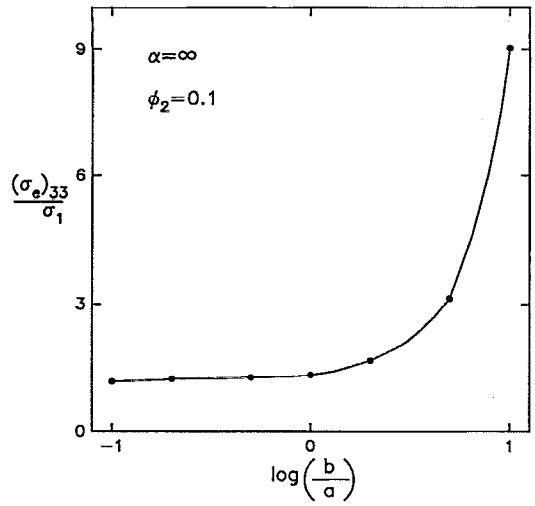

FIG. 13. The dimensionless 33 component of the effective conductivity vs $\log(b/a)$ for superconducting spheroids with $\phi_2=0.1$. Circles are our data and solid line is a spline fit of the data.

$$\tau_1(a+\delta_O,b+\delta_O)-\tau_1(a,b) \tag{A1}$$

since it takes no time to first hit the interface boundary. Although it is not clear that the resultant composite is exactly of spheroidal shape, it is enough to assume so for all practical purposes since δ_O is very small compared to a or b. Furthermore, $\tau_1(a+\delta_O,b+\delta_O)$ can be approximated by

$$\tau_1(a+\delta_O,b+\delta_O)\simeq\tau_1[a+\delta_O,b/a(a+\delta_O)]$$
$$=\tau_1(a,b)(1+\delta_O^2/a^2) \tag{A2}$$

for the same reason.

Consider next a Brownian particle *inside the concentric shell* of the composite spheroid described above (as in Fig. 2) such that the distance δ_I to the surface of the inner superconducting spheroid is very small compared to the shell thickness δ_O ($0\leqslant\delta_I<\delta_O<a$). Since such a Brownian particle can be alternatively considered to have already traveled from the centroid of the composite spheroid to the outer surface of another concentric shell of thickness δ_I and therefore the amount of time $\tau_1(a+\delta_I,b+\delta_I)-\tau_1(a,b)$ required for such a first-passage trip should be subtracted from the quantity (A1) in order to obtain the mean hitting time τ_s, then τ_s for this Brownian particle can be computed by

$$\tau_s=\tau_1(a+\delta_O,b+\delta_O)-\tau_1(a+\delta_I,b+\delta_I)$$
$$\simeq\tau_1(a,b)(\delta_O^2-\delta_I^2)/a^2. \tag{A3}$$

Equation (A3) in conjunction with the Table I for values of $\tau_1(a,b)$ was used in computation of the effective conductivity tensor for superconducting spheroids. The authors[8] earlier provided an expression for τ_s which is designed for use in cases of arbitrary shape of inclusions. Comparison of Eq. (A3) and their expression reveals that the latter slightly overestimates τ_s, leading to a slight overestimation of the effective conductivity.

Now to compute $\tau_1(a,b)$, consider a Brownian particle in a *nonsuperconducting, homogeneous* spheroid of semiaxes a and b, having conductivity σ_1. The mean hitting time $t(x)$ of such a Brownian particle initially at an arbitrary position x inside the spheroid to first hit the surface is given as the solution of a differential equation,[8]

$$\sigma_1\nabla^2 t=-1, \tag{A4}$$

with a trivial boundary condition that t vanishes at the surface. We are interested in the quantity $\tau_1(a,b)$ which is defined to be the mean hitting time for a Brownian particle initially at the centroid of a spheroid of semiaxes a and b such that $\tau_1(a,b)=t(\text{centroid})$. The quantity $\tau_1(a,b)$ can be numerically obtained for an arbitrary value of b/a by the first-passage-time algorithm earlier provided by the authors,[11] the essence of which is described in Sec. II A. Table I shows our simulation data for $\tau_1(a,b)$ for the aspect ratios $b/a=10$, 5, 2, 0.5, 0.2, 0.1 as well as the exact value for $b/a=1$ corresponding to spheres $[\tau_1(a,a)=a^2/6\sigma_1]$. The data in the table are obtained by the first-passage-time algorithm with 10^6 Brownian particles.

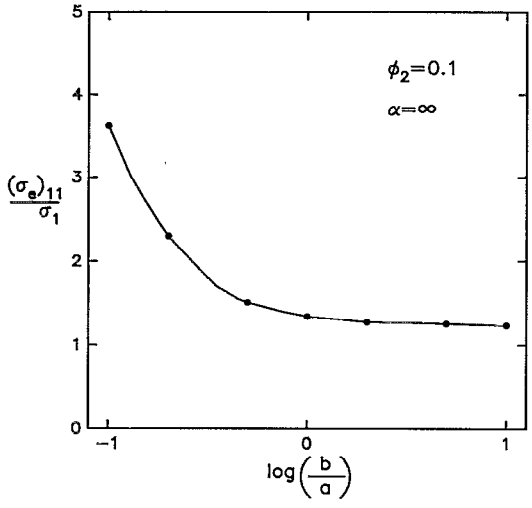

FIG. 14. The dimensionless 11 component of the effective conductivity vs $\log(b/a)$ for superconducting spheroids with $\phi_2=0.1$. Circles are our data and the solid line is a spline fit of the data.

[1] Z. Hashin, J. Appl. Mech. **50**, 481 (1983).
[2] G. W. Milton, Commun. Math. Phys. **111**, 281 (1987).
[3] S. Torquato, Appl. Mech. Rev. **44**, 37 (1991).
[4] J. R. Willis, J. Mech. Phys. Solids **25**, 185 (1977).
[5] A. Acrivos and E. S. G. Shaqfeh, Phys. Fluids **31**, 1841 (1988); E. S. G. Shaqfeh, Phys. Fluids **31**, 2405 (1988).
[6] A. K. Sen and S. Torquato, Phys. Rev. B **39**, 4504 (1989); S. Torquato and A. K. Sen, J. Appl. Phys. **67**, 1145 (1990).
[7] S. Y. Lu and S. Kim, AIChE J. **36**, 927 (1990).
[8] S. Torquato and F. Lado, J. Chem. Phys. **94**, 4453 (1991).
[9] I. C. Kim and S. Torquato, J. Appl. Phys. **68**, 3892 (1990).
[10] I. C. Kim and S. Torquato, J. Appl. Phys. **69**, 2280 (1991).

[11] I. C. Kim and S. Torquato, J. Appl. Phys. **71**, 2727 (1992).
[12] S. Torquato and I. C. Kim, Appl. Phys. Lett. **55**, 1847 (1989).
[13] N. Metropolis, A. W. Rosenbluth, M. N. Rosenbluth, A. N. Teller, and E. Teller, J. Chem. Phys. **21**, 1087 (1953).
[14] J. L. Lebowitz and J. W. Perram, Mol. Phys. **50**, 1207 (1983).
[15] C. A. Miller, I. C. Kim, and S. Torquato, J. Chem. Phys. **94**, 5592 (1991).
[16] S. B. Lee and S. Torquato, J. Chem. Phys. **89**, 3258 (1988).
[17] D. J. Bergman, Phys. Rep. **43**, 377 (1978); D. J. Bergman, Phys. Rev. Lett. **44**, 1285 (1980); G. W. Milton, J. Appl. Phys. **52**, 5294 (1981).